

PREPARED FOR THE U.S. DEPARTMENT OF ENERGY,
UNDER CONTRACT DE-AC02-76CH03073

PPPL-3632
UC-70

PPPL-3632

Resonant Plasma Heating Below the Cyclotron Frequency

by

Roscoe White, Liu Chen, and Zhihong Lin

November 2001



PRINCETON PLASMA PHYSICS LABORATORY
PRINCETON UNIVERSITY, PRINCETON, NEW JERSEY

PPPL Reports Disclaimer

This report was prepared as an account of work sponsored by an agency of the United States Government. Neither the United States Government nor any agency thereof, nor any of their employees, makes any warranty, express or implied, or assumes any legal liability or responsibility for the accuracy, completeness, or usefulness of any information, apparatus, product, or process disclosed, or represents that its use would not infringe privately owned rights. Reference herein to any specific commercial product, process, or service by trade name, trademark, manufacturer, or otherwise, does not necessarily constitute or imply its endorsement, recommendation, or favoring by the United States Government or any agency thereof. The views and opinions of authors expressed herein do not necessarily state or reflect those of the United States Government or any agency thereof.

Availability

This report is posted on the U.S. Department of Energy's Princeton Plasma Physics Laboratory Publications and Reports web site in Fiscal Year 2002. The home page for PPPL Reports and Publications is: http://www.pppl.gov/pub_report/

DOE and DOE Contractors can obtain copies of this report from:

U.S. Department of Energy
Office of Scientific and Technical Information
DOE Technical Information Services (DTIS)
P.O. Box 62
Oak Ridge, TN 37831

Telephone: (865) 576-8401
Fax: (865) 576-5728
Email: reports@adonis.osti.gov

This report is available to the general public from:

National Technical Information Service
U.S. Department of Commerce
5285 Port Royal Road
Springfield, VA 22161

Telephone: 1-800-553-6847 or
(703) 605-6000
Fax: (703) 321-8547
Internet: <http://www.ntis.gov/ordering.htm>

Resonant Plasma Heating Below The Cyclotron Frequency

Roscoe White¹, Liu Chen², Zhihong Lin¹

¹*Plasma Physics Laboratory, Princeton University, P.O.Box 451,*

Princeton, New Jersey 08543

²*Department of Physics and Astronomy, University of California, Irvine CA. 92697*

Abstract

Resonant heating of a magnetized plasma by low frequency waves of large amplitude is considered. It is shown that the magnetic moment can be changed nonadiabatically by a single large amplitude wave, even at frequencies normally considered nonresonant. Two examples clearly demonstrate the existence of the resonances leading to chaos and the generic nature of heating below the cyclotron frequency. First the classical case of an electrostatic wave of large amplitude propagating across a confining uniform magnetic field, and second a large amplitude Alfvén wave, propagating obliquely across the magnetic field. Waves with frequencies a small fraction of the cyclotron frequency are shown to produce significant heating; bringing, in the case of Alfvén waves, particles to speeds comparable to the Alfvén velocity in a few hundred cyclotron periods. Stochastic threshold for heating occurs at significantly lower amplitude with a perturbation spectrum consisting of a number of modes. This phenomenon may have relevance for the heating of ions in the solar corona as well as for ion heating in some toroidal confinement fusion devices.

PACS numbers: 52.35.Fp 52.50.Gj

I. Introduction

Resonant heating of particles in a magnetic field is a subject which has been examined by many authors and is of importance in the heating of magnetically confined laboratory as well as extraterrestrial plasmas. For a review see Lichtenberg and Lieberman.¹ It has been found that it is also possible to break the invariance of the magnetic moment at frequencies well below the cyclotron frequency.²⁻⁷ This phenomenon is due to the nonlinear coupling of higher harmonics of the guiding center motion with the cyclotron motion, and must be expected to occur for a large amplitude wave of almost any type. It is most easily analyzed by considering the classic case of an electrostatic wave propagating across a constant magnetic field.

The Alfvén wave is a fundamental excitation of a magnetically confined plasma. Alfvén waves, either excited spontaneously or by external sources, have been observed or predicted to be present in plasmas with parameters ranging from those of laboratory to space and astrophysical environments. Interactions between Alfvén waves and charged particles thus play crucial roles in many plasma dynamical processes. Pitch angle scattering and energization of charged particles (ions) by large amplitude Alfvén waves occurs at frequencies well below the cyclotron frequency Ω_c through a mechanism entirely analogous to that described by an electrostatic wave. Previous theoretical investigations of heating mechanisms have nearly always been based on the existence of the primary cyclotron resonance, which can change the magnetic moment leading to pitch angle scattering and heating. We have recently found⁷ that given a sufficiently large amplitude, obliquely propagating wave there indeed exists efficient stochastic ion pitch angle scattering and heating by the Alfvén wave even when $\omega \ll \Omega_c$.

We divide the presentation into a discussion of the standard model of electrostatic cyclotron heating in section II, higher order Hamiltonian analysis in Section III, heating with Alfvén waves in section IV, and conclusions in Section V.

II. Electrostatic Cyclotron Heating

Consider the simplest cyclotron heating problem possible¹, that of a particle gyrating in a constant magnetic field, acted upon by an electrostatic plane wave propagating across the field. This situation is realizable for example by a lower hybrid wave in a plasma of high density and small magnetic field, propagating perpendicularly to \vec{B} at the ion plasma frequency. The observation of stochastic heating has in fact been reported in work we only recently discovered.⁴ We will find that the resonances producing stochastic heating below the cyclotron frequency occur through the same mechanism as those due to any wave in a magnetized plasma, so this model illustrates the heating mechanism well.

The Hamiltonian for this system is

$$H = \frac{(\vec{p} - \vec{A})^2}{2} + \Phi(x, t) \quad (1)$$

with the magnetic field given by the vector potential $\vec{A} = -By\hat{x}$, giving equations of motion $\dot{v}_x = Bv_y - \partial_x\Phi$, $\dot{v}_y = -Bv_x - \partial_y\Phi$.

Take the units of time to be given by Ω_c , the cyclotron frequency, and let the electrostatic wave be given by a single harmonic, $\Phi = \Phi_0 \cos(kx - \omega t)$. There are then three dimensionless parameters characterizing the heating problem. Define $\rho = v/\Omega_c$ to be the instantaneous cyclotron radius. Then $k\rho$ characterizes the ratio of cyclotron radius to wave length, $k^2\Phi_0 = k\Delta x_g = \omega_b^2/\Omega_c^2$ characterizes the ratio of guiding center polarization drift displacement in the wave to wave length, with ω_b the bounce frequency in the wave and x_g the guiding center position, and ω/Ω_c gives the ratio of the wave frequency to the cyclotron frequency.

The equations of motion become, $\dot{v}_x = v_y + k\Phi_0 \sin(kx - \omega t)$, $v_y = -x + x_0$, giving

$$\frac{d^2x}{dt^2} + x = x_0 + k\Phi_0 \sin(kx - \omega t). \quad (2)$$

It is easy to see that trapping in the wave is impossible, prevented by the cyclotron motion. During each cyclotron period, at the point $v_y = 0$ the orbit returns to the point x_0 and every orbit is thus fixed in the laboratory frame. Conversely, assuming that the

orbit is trapped in the wave with $kx \simeq \omega t$ we find that v_y grows without bound, which is inconsistent with trapping.

For small wave amplitude at the cyclotron frequency it is possible to describe the particle response to the wave in terms of oscillation at the cyclotron frequency with a slowly varying cyclotron radius, or energy. In the case of interest here wave amplitudes are large and wave frequencies different from, but comparable to, the cyclotron frequency, so response of the particle at additional frequencies must be retained. To treat the full problem it is necessary to include particle motion at fractions of the cyclotron frequency, sidebands, harmonics, etc. The particle motion must be written $x = x_0 + \lambda \cos(t) - \alpha \sin(t) + \sum_m [\alpha_m \cos(\nu_m t) + \beta_m \sin(\nu_m t)]$ with $\lambda, \alpha, \alpha_m, \beta_m$ slowly varying in time compared to $1, \nu_m$, and ν_m giving the set of frequencies necessary to describe the motion. A full analytic treatment is not possible, but some analytic approximations give insight into the nature of the solutions.

First consider Eq. 2 for $s \equiv k(x - x_0) \ll 1$. Letting $2T = kx_0 - \omega t$ and keeping only lowest order in s we have

$$\frac{d^2 s}{dT^2} + \left[\frac{4}{\omega^2} - \frac{4k^2 \Phi_0}{\omega^2} \cos(2T) \right] s = \frac{4k^2 \Phi_0}{\omega^2} \sin(2T) \quad (3)$$

ie, a driven Mathieu equation. This equation has unstable solutions for $\omega \simeq 2/N$ with N integer, indicating the existence of large amplitude solutions for these values of ω .

Now consider a Poincaré section of $k\rho, \psi = kx - \omega t$, by taking points when $v_y = 0, \dot{v}_y > 0$. This gives $\psi = \psi_0 - \omega t_j$, with $\psi_0 = kx_0$, and t_j given by the times at which $x = x_0$ and $\dot{x} < 0$. Given $\lambda(t), \alpha(t), \alpha_m(t), \beta_m(t)$ one can solve for the Poincaré times t_j . Without loss of generality we take at $t = 0$ initial values x random, v_x random negative and $v_y = 0$, giving $x = x_0, \psi(0) = \psi_0$. The values at $t = 0$ then determine one Poincaré point. Others are given by $k\rho(t_j), \psi(t_j) = \psi_0 - \omega t_j$. Fixed points are given by $dv/dt = 0$ and constant phase, or $\dot{\lambda} = \dot{\alpha} = \dot{\alpha}_m = \dot{\beta}_m = 0$.

In general these equations are very complicated and the Poincaré section must be examined numerically. For significant heating there must exist resonances. A complete analysis would consist of a determination of all fixed points and then the calculation of the widths of

the islands occuring around the elliptic points, followed by an estimate of stochastic threshold due to island overlap. Unfortunately this approach is not feasible, and to make any progress analytically one must be guided by numerical results. A numerical Poincaré plot is shown in Fig. 1 for $k^2\Phi_0 = 0.1$, $\omega = 1/2$, showing period two fixed points occuring at small wave amplitude. In Fig. 2 are shown these two fixed point orbits, the smaller orbit to the left corresponding to the lower fixed points at $k\rho \simeq 0.825$, $\psi = 0, \pi$, and the larger corresponding to the upper fixed points at $k\rho \simeq 1.841$, $\psi = \pm\pi/2$. The nature of the resonance is obvious, a particle at the fixed point completes two cyclotron periods while completing one wave period. The first fixed point orbit shows a large variation of the orbit between one cyclotron period and the second, in the second orbit this modification is clearly higher order.

Guided by numerical results, including a Fourier analysis of the fixed point trajectories, we illustrate the nature of the solutions for this case by considering only the cyclotron motion and the particle response at the wave frequency of $\omega = 1/2$. Employing multiple time scales, and using as ansatz the solution to the equations of motion $x = x_0 + \lambda\cos(t) - \alpha\sin(t) - \beta\sin(\omega t)$ with λ, α, β slowly varying with respect to $1, \omega$, we then find, keeping only leading order in the slow time scale and using $e^{\pm ia\sin(b)} = \sum_m J_m(a)e^{\pm imb}$,

$$\begin{aligned}
& -2\frac{d\alpha}{dt}\cos(t) - 2\frac{d\lambda}{dt}\sin(t) - (1 - \omega^2)\beta\sin(\omega t) = \\
& k\Phi_0 \sum_{jlm} J_j(k\lambda)J_l(k\alpha)J_m(k\beta)\sin[(j - l - m\omega - \omega)t]\cos[\psi_0 + j\pi/2] \\
& + k\Phi_0 \sum_{jlm} J_j(k\lambda)J_l(k\alpha)J_m(k\beta)\cos[(j - l - m\omega - \omega)t]\sin[\psi_0 + j\pi/2].
\end{aligned} \tag{4}$$

Integrating over the short time scales, we have

$$(1 - \omega^2)\beta = k\Phi_0 \sum_{jlm} J_j(k\lambda)J_l(k\alpha)J_m(k\beta)\cos(\psi_0 + j\pi/2)\Delta_{\omega-}, \tag{5}$$

$$2\frac{d\alpha}{dt} = -k\Phi_0 \sum_{jlm} J_j(k\lambda)J_l(k\alpha)J_m(k\beta)\sin(\psi_0 + j\pi/2)\Delta_{1+}, \tag{6}$$

$$2\frac{d\lambda}{dt} = -k\Phi_0 \sum_{jlm} J_j(k\lambda)J_l(k\alpha)J_m(k\beta)\cos(\psi_0 + j\pi/2)\Delta_{1+}, \tag{7}$$

with $\Delta_{\zeta\pm} = \delta_{j-l+(-m-1)\omega,\zeta} \pm \delta_{j-l+(-m-1)\omega,-\zeta}$.

To gain an intuitive understanding of the occurrences of the nonlinear resonances which permit heating at frequencies well below the cyclotron frequency, we can examine the limit of small wave amplitude, $k^2\Phi_0 \ll 1$, analytically for $\omega = 1/2$. Denoting $C_0 = \cos(\psi_0)$, $S_0 = \sin(\psi_0)$, and defining $F_{a,b}(\lambda, \alpha) = \sum_{n=-\infty}^{\infty} (-1)^n J_{2n+a}(k\lambda) J_{2n+b}(k\alpha)$, we find

$$(1 - \omega^2)\beta = k\Phi_0[C_0(F_{0,0} - F_{0,-1}) + S_0(F_{1,0} - F_{1,1})], \quad (8)$$

$$2\frac{d\alpha}{dt} = k\Phi_0 J_1(k\beta)[C_0(F_{1,0} - F_{1,-1} + F_{1,2} - F_{1,1}) + S_0(F_{0,-1} - F_{0,-2} + F_{0,1} - F_{0,0})], \quad (9)$$

$$2\frac{d\lambda}{dt} = k\Phi_0 J_1(k\beta)[S_0(-F_{1,0} + F_{1,-1} + F_{1,2} - F_{1,1}) + C_0(F_{0,-1} - F_{0,-2} - F_{0,1} + F_{0,0})]. \quad (10)$$

Within this ansatz, these equations determine the motion of a Poincaré point in the $k\rho$, ψ plane for small $k^2\Phi_0$. To determine the existence of resonances first look for fixed points of the Poincaré map. In this case $k\beta$ and $k\lambda$ are small and we find for the existence of a fixed point in the case $\omega = 1/2$, $C_0 = 1$, $S_0 = 0$ and $\lambda = 0$, $J_0(k\alpha) = 2J_1(k\alpha) + J_2(k\alpha)$ giving $k\alpha = 0.825$ and $\beta = -1.62k\Phi_0$. The Poincaré points are given by $t_j = 2j\pi$. The fixed points are then $k\rho = k(\alpha - \omega\beta)$, $\psi = 0$ and $k\rho = k(\alpha + \omega\beta)$, $\psi = \pi$, agreeing with the positions shown in Fig. 1. The second pair of fixed points in Fig. 1 at $\psi = \pm\pi/2$ and $k\rho = 1.84$, giving the larger orbit in Fig. 2 is more complex, due to a combination of higher order motion at ω and 3ω . Including particle response at more frequencies, and allowing larger values of $k^2\Phi_0$ the number of fixed points in the map increases enormously.

For $\omega \neq 1/2$ but less than 1, the situation is qualitatively different. The fixed points of the map emerge from $\rho = 0$ as Φ_0 is increased. Nevertheless, fixed points and resonances exist for all integer N , associated with the unstable domains of the associated Mathieu equation. In the following we show a few of the Poincaré plots and associated fixed point orbits to make clear the nature of the resonances involved producing stochastic heating.

A numerical Poincaré plot is shown in Fig. 3 for $k^2\Phi_0 = 0.1$, $\omega = 1/3$, showing period three fixed points which move upward as $k^2\Phi_0$ increases. In Fig. 4 is shown the fixed

point orbit for $\omega = 1/3$. The motion is easily interpreted as consisting of three cyclotron oscillations within one wave period. The orbit initiates at the origin, which is one Poincaré point, with $\dot{x} < 0$. The three cyclotron periods consist of 1) the left half of the lower ellipse, continuing around to the bottom of the small central ellipse, which is another Poincaré point, 2) the upper ellipse, returning again to the bottom of the small central ellipse, which is the third Poincaré point, and 3) the right half of the lower ellipse, returning to the origin.

In Fig. 5 is shown the Poincaré plot for $\omega = 1/4$, $k^2\Phi_0 = 0.77$, and in Fig. 6 is shown the period four fixed point orbit associated with the fixed points at $\psi = 0, \pm\pi/2, \pm\pi$ for the same parameters. There are four cyclotron periods contained in the wave period. The map has also become very chaotic, but good KAM surfaces exist for $k\rho > 2$.

For $\omega = 2/N$ with N odd the fixed point orbit is not simply interpretable as consisting of an integer number of cyclotron periods in one wave period, as the cases with ω equal to a simple fraction. Part of the orbit has a peculiar shape and consists of a pause, or syncopation, allowing one wave period for every $N/2$ cyclotron periods.

In the above figures, the fixed point orbits are shown only to display the nature of the resonances. Most orbits are obviously very complex, and are not closed. The nature of these resonances is very robust. Small additional perturbations of the system shift the location of the O-points, they do not destroy the resonances. Even including pitch angle scattering in the particle motion the resonances are well preserved until the scattering frequency is comparable to the cyclotron frequency.

Now investigate the approach to chaos and the extent of the chaotic domain, which limits the possible heating obtained. Stochastic threshold is not simply described in terms of island overlap, as is evident from Fig. 1. The islands at small perturbation amplitude are already large, forming a lattice. For frequencies below the cyclotron frequency the resonance domain, and hence the origin of the chaos, is at small energies, unlike the case of heating well above the cyclotron frequency.⁸ The stochastic domain typically extends from $\rho = 0$ to a maximum value, where good KAM surfaces exist and the perpendicular energy is only oscillatory, described by the magnetic moment. The extent of the stochastic domain

increases in discrete jumps as new resonances overlap and domains around them become stochastic. Heating of an initially cold distribution proceeds to the maximum limit given by the good KAM surfaces in a rather short time; on the order of one to two hundred cyclotron periods.

Figure 7 shows the variation of the extent of the “heating domain” in $k\rho$ versus wave frequency for $k^2\Phi_0 = 0.36, 0.8,$ and 2.6 . For small wave amplitude some peaking can indeed be seen at low-order (small) integer fractions, as predicted by the Mathieu equation approximation. As the amplitude increases, however, nonlinear generation of many fixed points produces chaos which smooths out the resonance structures and makes the extent of the domain almost linear in ω . Of course at small amplitude and in the limit of $\omega \rightarrow 0$ for any amplitude the motion is not stochastic, and there is no real heating, only large amplitude excursions in the potential. But for large amplitude the motion becomes stochastic, producing true heating, for very low frequencies. For the two larger amplitude plots an X indicates the frequency for the onset of chaos. For $k^2\Phi_0 = 0.36$, curve a, there is no chaos, only large scale convective motion, even at $\omega = 1$.

The onset of chaos at large wave amplitude as a function of ω is shown in Fig. 8. Note that heating at the cyclotron frequency has a threshold not significantly lower than for subcyclotron frequencies. Values of $k^2\Phi_0$ above the line give a significantly stochastic plot, with the area of the domain of stochasticity increasing rapidly as one moves away from the line. The onset of chaos is very irregular, it can occur through period doubling, the overlap of islands of various period, or through the stochastic broadening of a separatrix.

III. Hamiltonian Analysis

The resonances described above are missed in the usual Hamiltonian formalism. To see how this occurs follow Lichtenberg and Lieberman.¹ The unperturbed Hamiltonian is $H_0 = (\vec{p} - \vec{A})^2/2$ with $\vec{B} = B\hat{z}$, the vector potential $\vec{A} = \Omega_c x \hat{y}$, and canonical variables x, y, p_x, p_y . Transform to guiding center variables ϕ, X, P_X, P_ϕ using $F_1(q, Q, t) = \Omega_c [\frac{1}{2}(x - X)^2 \cot\phi +$

$yX]$, with $\tan\phi = v_x/v_y$, $y = Y + \rho\cos\phi$, $x = X + \rho\sin\phi$, $p = \partial F_1/\partial q$, $P = -\partial F_1/\partial Q$, giving $p_x = \Omega_c(x - X)\cot\phi$, $p_y = \Omega_c X$, $P_\phi = \Omega_c \rho^2/2$, $P_X = -\Omega_c Y$. Then we have $H_0 = P_\phi \Omega_c$. Now introduce the perturbation $H = H_0 + \Phi_0 \sin(kx - \omega t)$. Make the transformation $X, P_X \rightarrow \psi, P_\psi$ with $\psi = kX - \omega t$ using $F_2(q, P, t) = (kX - \omega t)P_\psi + P_\phi \phi$, giving $p = \partial F_2/\partial q$, $Q = \partial F_2/\partial P$, $P_X = kP_\psi$, and the Hamiltonian becomes

$$H = P_\phi \Omega_c - P_\psi \omega + \Phi_0 \sum_m J_m(k\rho) \sin(\psi + m\phi) \quad (11)$$

with variables $\psi, \phi, P_\psi, P_\phi$ and unperturbed frequencies $\omega_\phi = \partial_{P_\phi} H_0 = \Omega_c$, $\omega_\psi = \partial_{P_\psi} H_0 = -\omega$.

The first order perturbation gives resonances, with a secularity of the perturbation, when $\psi + m\phi = \text{constant}$, or $\omega - m\Omega_c = 0$, *ie* the usual cyclotron harmonics. But if Φ_0 is large, this analysis is incomplete. To obtain higher order in Φ_0 , begin with Eq. 2. Take $\omega \ll 1$, and perform a two time scale analysis with $X(t)$ slow. Neglecting slow time scale dependence, and averaging over the fast time scale we find $kX = kx_0 + k^2 \Phi_0 \langle \sin(kX + k\rho \sin\phi - \omega t) \rangle$. Again transform $X, P_X \rightarrow \psi, P_\psi$ using $F_2(q, P, t)$ as above. Then find the equation for ψ to be $\psi = \psi_0 + k^2 \Phi_0 \langle \sin(\psi + k\rho \sin\phi) \rangle$ with $\psi_0 = kx_0 - \omega t$. Now iterate twice in powers of $k^2 \Phi_0$ giving $\psi_2 = \psi_0 + k^2 \Phi_0 \sum_m J_m(k\rho) \langle \sin(\psi_0 + m\phi) \rangle + (k^4 \Phi_0^2/2) \sum_{mn} J_m(k\rho) J_n(k\rho) \langle \sin(2\psi_0 + m\phi + n\phi) \rangle + (k^4 \Phi_0^2/2) \sum_{mn} J_m(k\rho) J_n(k\rho) \langle \sin(m\phi - n\phi) \rangle$.

Recall the Hamiltonian is $H = H_0 + \Phi_0 \sin(\psi + k\rho \sin\phi)$, so $\langle k^2 H \rangle \sim \psi$. But terms in ψ_2 with $m + n = 1$ give a secularity at $2\omega = \Omega_c$. To find the secularities at $\omega = \Omega_c/N$ it is necessary to perform N iterations, and the Hamiltonian becomes very complicated. Furthermore this is a $\omega \ll \Omega_c$ approximation, and cannot even reproduce the case $\omega = \Omega_c/2$ described above, with any degree of accuracy.

IV. Alfvén wave Heating

Now examine stochastic heating of cold ions by low frequency Alfvén waves. The physics of this stochastic heating is similar to that due to a perpendicularly propagating electrostatic

wave with a frequency a small fraction of Ω_c given above.⁷ To demonstrate the similarity consider a linearly polarized Alfvén wave in the laboratory frame X, Y, Z , given by $\vec{B}_w = B_w \hat{y} \cos(\psi)$ with $\psi = \vec{k} \cdot \vec{X} - \omega t$ and $\vec{B} = B_0 \hat{z}$. We have $\omega = k_z v_A$ and if we consider ions which are cold in the laboratory frame we have also $\omega = k_z v_A = k_z v$ with v the velocity in the wave frame x, y, z with $z = Z - v_A t$. Take the units of time to be given by Ω_c , the cyclotron frequency, and normalize the field to B_0 . In the wave frame we have $\psi = k_x x + k_z z$ and the velocity $v = v_A$ is constant in time. Dimensionless numbers characterizing the problem are then $k_x v$, $k_z v = \omega/\Omega_c$, and the wave magnitude B_w/B_0 .

The equations of motion become, again in the wave frame, $\dot{v}_x = v_y - v_z B_w \cos \psi$, $v_y = x_0 - x$, $\dot{v}_z = v_x B_w \cos \psi$, giving

$$\frac{d^2 x}{dt^2} + x = x_0 - v_z B_w \cos \psi \quad (12)$$

and the instantaneous location of a particle in phase space is given by x, z and the pitch $\lambda = v_z/v$. Note that $v_y = 0$ implies again $x = x_0$ and every orbit is thus localized in x , but in distinction to the electrostatic case the wave is also propagating in z .

To lowest order in B_w , the velocity v_z does not change, and we thus find to first order $d^2 x/dt^2 + x = x_0 - v_z(0) B_w \cos \psi$. This equation is equivalent to Eq. 2, describing cyclotron heating, with $\omega/\Omega_c = k_z v_z(0)/\Omega_c$ playing the role of the frequency of the electrostatic wave, and $k_x v_z(0) B_w / (B_0 \Omega_c)$ the nonlinearity parameter. We again find a driven Mathieu equation with unstable solutions for $\omega \simeq 2/N$ with N integer. Thus there are resonances at many values of particle pitch in the wave frame. However, note that $k_x = 0$ implies no nonlinear interaction, so we expect nonlinear effects only for waves propagating across the field. For larger values of B_w the approximation of $v_z = v_z(0)$ will be invalid in the differential equation for x and the motion will be more complex. Thus we expect the threshold for chaos to occur at lower perturbation amplitude than for the case of an electrostatic wave.

To study the resonances, again take a Poincaré section of λ, ψ , formed by taking points when $v_y = 0$ and $\dot{v}_y > 0$ for a distribution at a fixed energy, *ie* all particles with the same v in the wave frame. Figure 9 shows a sample Poincaré plot with $k_x v = 0.1$, $k_z v = 1$,

$B_w = 0.22$, with resonances at $k_z v_z = 2/n$ for all integer $n \geq 2$, although only a few are visible in this plot. Large islands centered at zero pitch are populations of particles trapped in the magnetic well. In a way, the Alfvén problem is simpler than the electrostatic problem, because the location of the resonances in the Poincaré plot in this case is known. At larger wave amplitude these resonances produce stochastic motion, and hence allow non adiabatic, permanent change in pitch λ . Transformed back to the laboratory frame such a change in pitch is equivalent to particle acceleration and heating as well as pitch angle scattering.

Noting that waves of left hand polarization are often excited in space plasmas, we shall consider in the following only a left hand circularly polarized Alfvén wave. Thus we have, again in the wave frame $\vec{B}_w = -B_w \hat{x} \cos(\alpha) \sin(\psi) + B_w \hat{y} \cos\psi + B_w \hat{z} \sin(\alpha) \sin(\psi)$ with $\psi = k_x x + k_z z$ and $\tan(\alpha) = k_x/k_z$. In the laboratory frame the wave propagates in the positive z direction, and in the wave frame $v_z/v = -1$ for an initially cold ion distribution. Figure 10 shows a Poincaré plot for a left hand circularly polarized wave with $B_w = 0.25$, $k_x v = 0.27$, $k_z v = 0.2$. In the laboratory frame of the cold particles this wave has a frequency of $\omega/\Omega_c = 0.2$. At this amplitude the lower part of the plot is chaotic, and ions can freely move from $v_z/v = -1$ to values near -0.4 , but above this there are good KAM surfaces. Transforming back to the laboratory frame, the final ion distribution has a mean perpendicular velocity more than three times as large as the mean parallel velocity. An initially cold distribution is given a large perpendicular energy in a few hundred cyclotron periods.

In Fig. 11 is shown a numerical determination of the stochastic threshold in the plane of $k_x v, B_w$ for frequencies of $\omega/\Omega_c = 0.1, 0.25, 0.5$. This plot was obtained by observing the Poincaré plot of initially cold (pitch = -1) particles. Above the line there is a significant chaotic domain leading to heating, and below it good KAM surfaces exist, preventing heating.

With a spectrum consisting of waves of different frequencies a Poincaré plot cannot be used to investigate the onset of chaos. However it is possible to examine the presence of chaos by using a perturbation which is Gaussian in time, tending to zero at $t = \pm\infty$ with a

width of $\delta t \gg 1/\Omega_c$. In Fig. 12 is shown the adiabatic nature of the particle energy change for a small amplitude perturbation, with a spectrum of 21 modes all with $k_x V_a = k_z V_a = \Omega_c$, uniformly distributed in the interval $0.2 < \omega/\Omega_c < .7$, the amplitude for mode k given by $\delta B_k \sim A/\omega_k$, as suggested by solar corona spectroscopy.⁹ The initial particle distribution was monoenergetic with $v = V_A/20$ and uniform in pitch. Over 90 percent of the energy is in the perpendicular velocity, so these plots are essentially of the magnetic moment. In Fig. 13 is shown the nonadiabatic response with a larger amplitude perturbation. Figure 14 gives the final energy change as a function of average mode amplitude for spectra consisting of 1, 5, 21, and 51 modes with $k_x V_A = 1$ and one spectrum with $k_x V_A = 10$, all in the frequency range $0.2 < \omega/\Omega_c < .7$, showing an approximate threshold behavior. As expected from the linear analysis, larger k_x increases the level of chaos. There is not a precise threshold for heating because as δB increases small chaotic domains begin to appear, with a few particles affected. However above a fairly well defined point almost all of phase space is stochastic up to some limiting energy, and the whole distribution is heated irreversibly. Within limits, extending the width of the Gaussian perturbation does not change results, the particles are heated up to the limiting KAM surface in a few hundred cyclotron periods. The stochastic threshold and the amount of heating depend on the properties of the spectrum in ways which are still being investigated.

V. Conclusion

In conclusion, we have demonstrated that significant perpendicular heating of a magnetized plasma can be obtained well below the cyclotron frequency. The example of an electrostatic wave propagating across a constant magnetic field with a frequency below the cyclotron frequency serves as a simple mathematical model for the effect. The resonances involve orbits which complete multiple cyclotron periods in one wave period. Stochastic threshold for a single wave occurs at an amplitude which is almost independent of the wave frequency, and in the presence of several waves the threshold is significantly lowered. This generic

process is due to the nonlinear coupling of the motion of the guiding center due to the wave with the cyclotron motion, and can occur with any type of wave. The process may have application in laboratory heating devices as well as in astrophysical situations. Of particular interest is a spectrum of Alfvén waves, which can energize cold ions even when the wave frequency is well below the ion cyclotron frequency. This effect may be of importance in the heating of ions in the solar corona⁷ and in transferring energy directly from a fast ion population to bulk thermal ions in a magnetically confined toroidal plasma with low aspect ratio.¹⁰

This work was supported by the U.S. Department of Energy Grant DE-FG03-94ER54271 and under contract number DE-AC02-76-CHO3073 and NSF Grant ATM-9971529. The authors acknowledge useful discussions with Fulvio Zonca, Dave Gates, Nikolai Gorelenkov, Stan Kaye, Eric Fredrickson, and Ron Bell.

REFERENCES

1. M. A. Lieberman and A. J. Lichtenberg *Regular and Chaotic Dynamics* Springer Verlag, New York (1983) p 87.
2. Yu. N. Smirnov and D. A. Frank-Kamenetskii *Sov. Phys. JETP*, **26**, 627 (1968).
3. T. Terasawa, M. Nambu *Geo. Res. Lett.* **16**, 357 (1989).
4. J. M. McChesney, P. M. Bellan, and R. A. Stern *Phys. Rev. Lett.* **59**, 1436 (1987).
5. A. D. Bailey, R. A. Stern, and P. M. Bellan *Phys. Plasmas* **2**, 2963 (1995).
6. J. R. Johnson and C. Z. Cheng *Private Communication* (2001).
7. L. Chen, Z. Lin and R. B. White *Phys. Plasmas* **8**, 4713 (2001).
8. C. F. F. Karney *Phys. Fluids* **22** 2188 (1979).
9. S. R. Cranmer, G. B. Field and J. L. Kohl *Astrophysical J.* **518**, 937 (1999).
10. D. Gates, N. Gorelenkov and R. B. White *Phys. Rev. Lett.* **87**, 205003-1 (2001).

Figure Captions

Fig. 1 Poincaré plot for Electrostatic wave, $k^2\Phi_0 = 0.1$, $\omega = 1/2$

Fig. 2 Fixed point orbits for Fig. 1

Fig. 3 Poincaré plot for Electrostatic wave, $k^2\Phi_0 = 0.1$, $\omega = 1/3$

Fig. 4 Fixed point orbit for Fig. 3

Fig. 5 Poincaré plot for Electrostatic wave, $k^2\Phi_0 = 0.77$, $\omega = 1/4$

Fig. 6 Fixed point orbit associated with Fig. 5

Fig. 7 Heating Domain vs ω for $k^2\Phi_0 =$ a) 0.36, b) 0.8 c) 2.6

Fig. 8 Threshold for chaos in the $k^2\Phi_0, \omega$ plane.

Fig. 9 Poincaré plot for a plane polarized Alfvén wave, $B_w = 0.22$, $k_x v = 0.1$, $k_z v = 1$.

Fig. 10 Poincaré plot for a circularly polarized Alfvén wave, $B_w = 0.25$. $k_x v = 0.27$, $k_z v = 0.2$.

Fig. 11 Stochastic threshold, (a) $\omega = 0.5$, (b) $\omega = 0.25$, (c) $\omega = 0.1$

Fig. 12 Energy time history for spectrum of Alfvén waves with $\delta B/B = 4 \times 10^{-3}$

Fig. 13 Energy time history for spectrum of Alfvén waves with $\delta B/B = 4 \times 10^{-2}$

Fig. 14 Stochastic heating due to a spectrum of Alfvén waves.

FIGURES

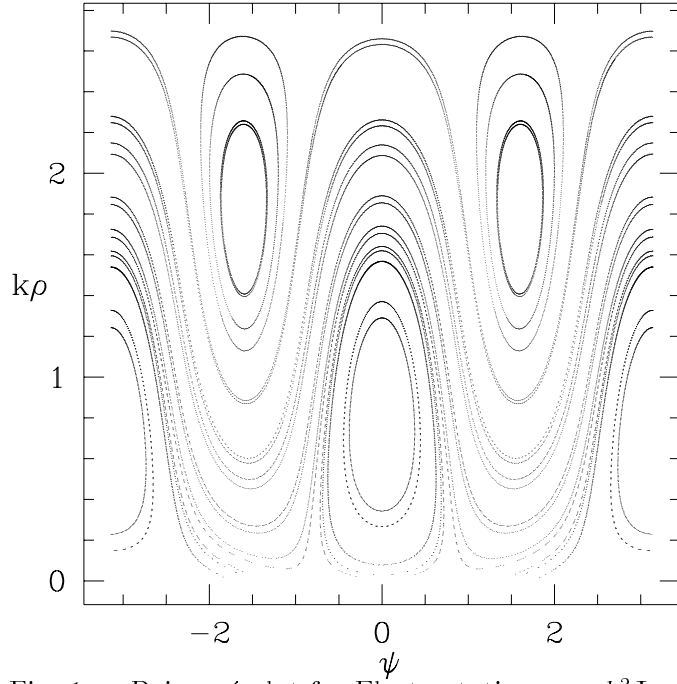


Fig. 1. Poincaré plot for Electrostatic wave, $k^2\Phi_0 = 0.1$, $\omega = 1/2$

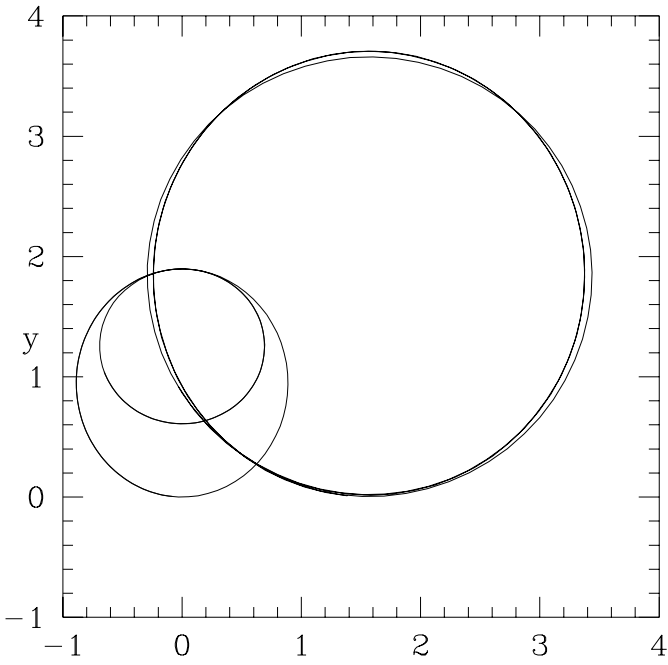


Fig. 2. Fixed point orbits for Fig. 1

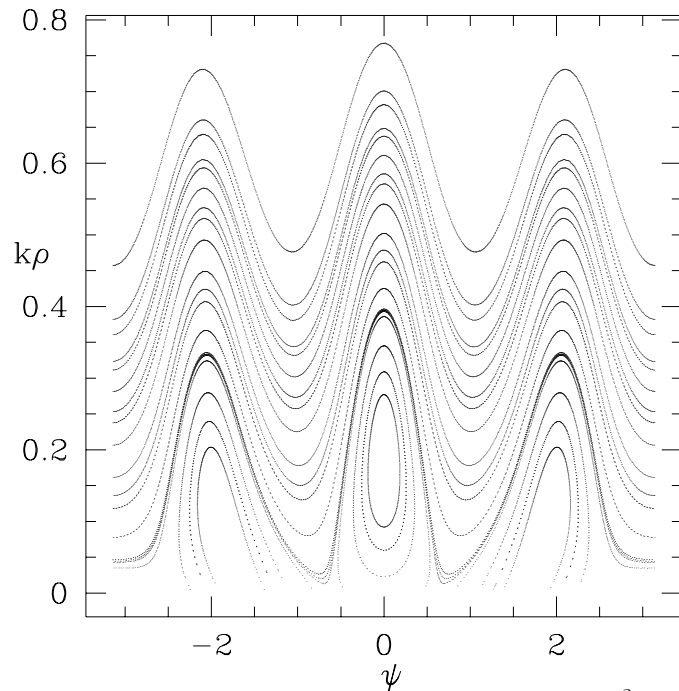


Fig. 3. Poincaré plot for Electrostatic wave, $k^2\Phi_0 = 0.1$, $\omega = 1/3$

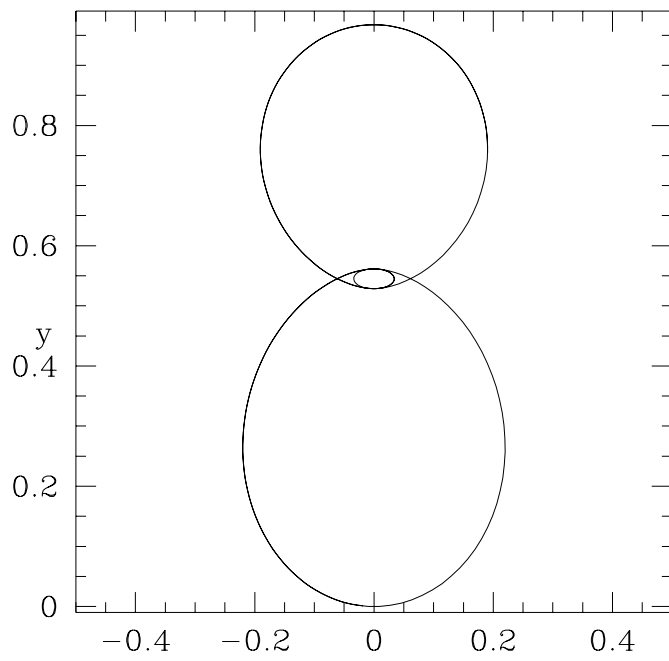


Fig. 4. Fixed point orbit for Fig. 3

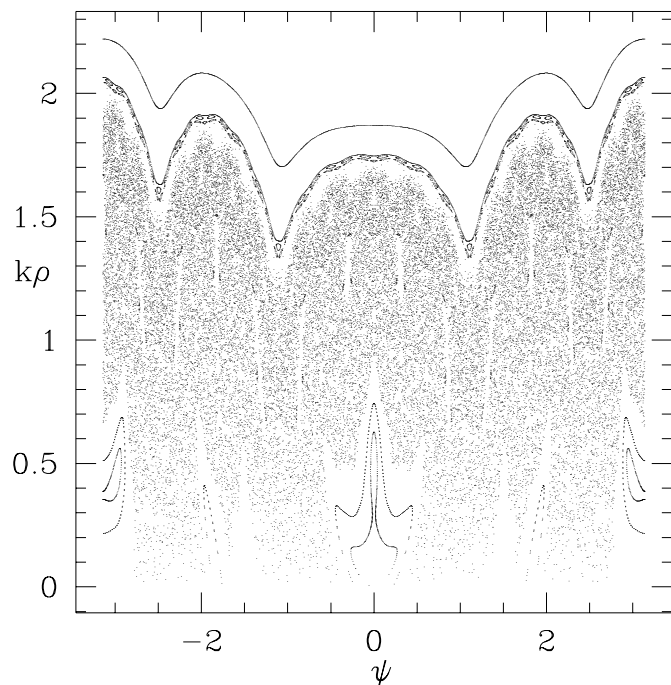


Fig. 5. Poincaré plot for Electrostatic wave, $k^2\Phi_0 = 0.77$, $\omega = 1/4$

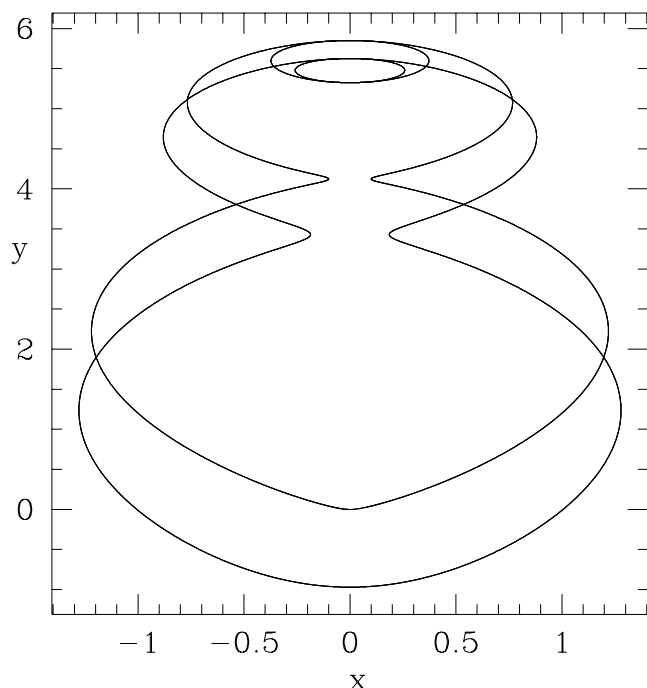


Fig. 6. Fixed point orbit associated with Fig. 5

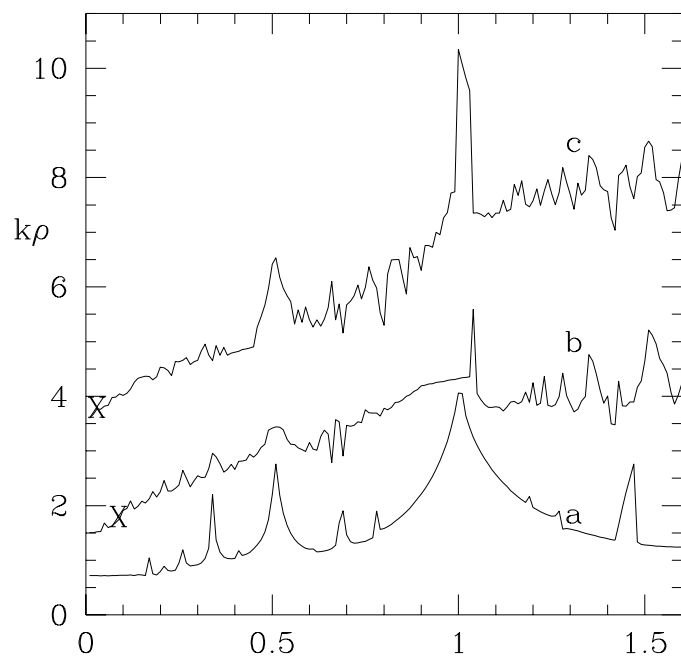


Fig. 7. Heating Domain vs ω for $k^2\Phi_0 =$ a) 0.36, b) 0.8 c) 2.6

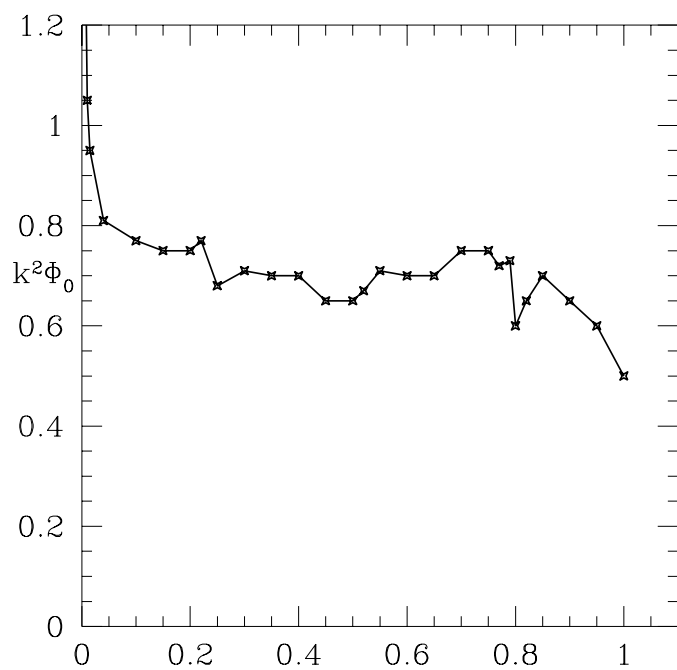


Fig. 8. Threshold for chaos in the $k^2\Phi_0, \omega$ plane.

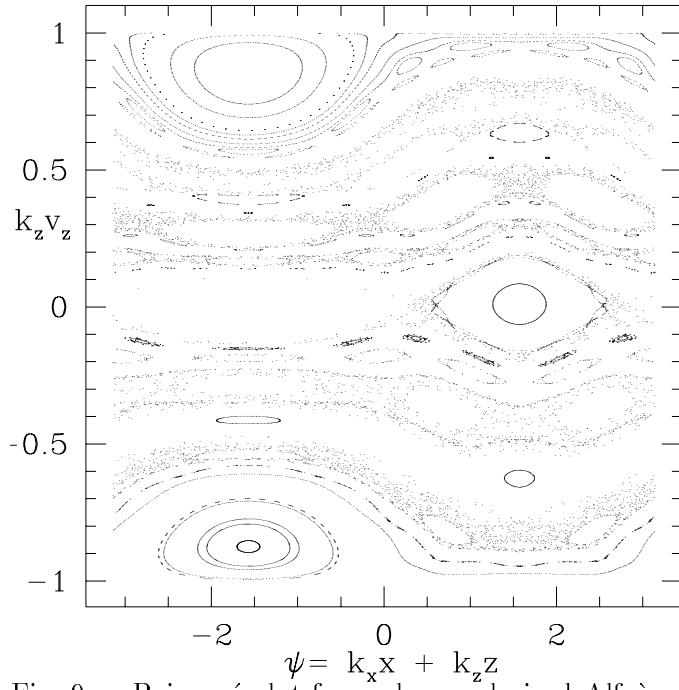


Fig. 9. Poincaré plot for a plane polarized Alfvén wave, $B_w = 0.22$, $k_x v = 0.1$, $k_z v = 1$.

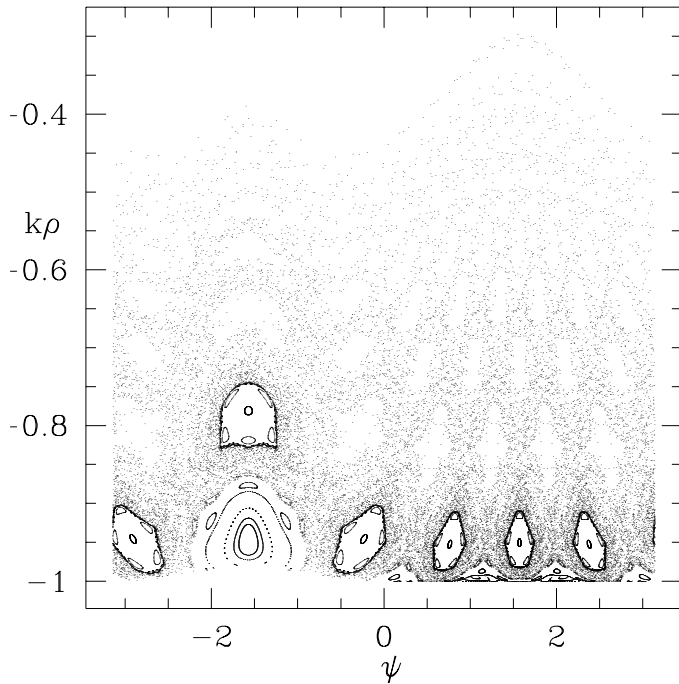


Fig. 10. Poincaré plot for a circularly polarized Alfvén wave, $B_w = 0.25$, $k_x v = 0.27$, $k_z v = 0.2$.

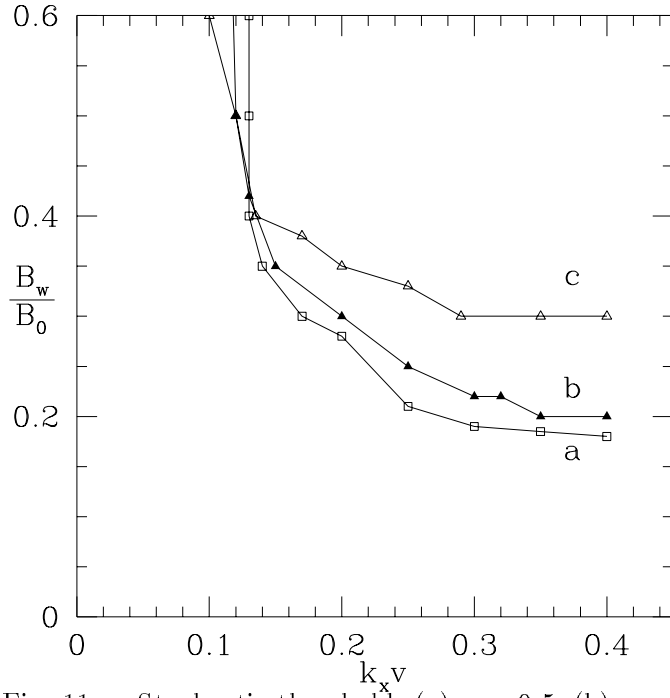


Fig. 11. Stochastic threshold, (a) $\omega = 0.5$, (b) $\omega = 0.25$, (c) $\omega = 0.1$

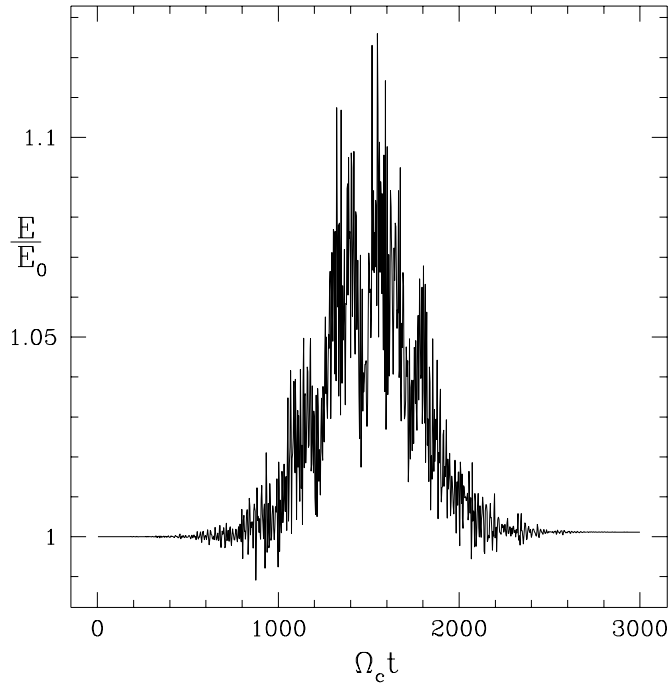


Fig. 12. Energy time history for spectrum of Alfvén waves with $\delta B/B = 4 \times 10^{-3}$

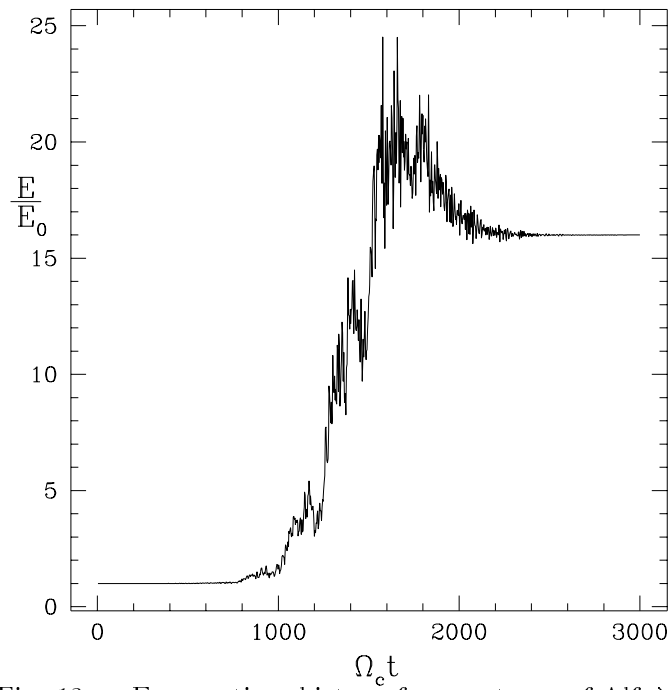


Fig. 13. Energy time history for spectrum of Alfvén waves with $\delta B/B = 4 \times 10^{-2}$

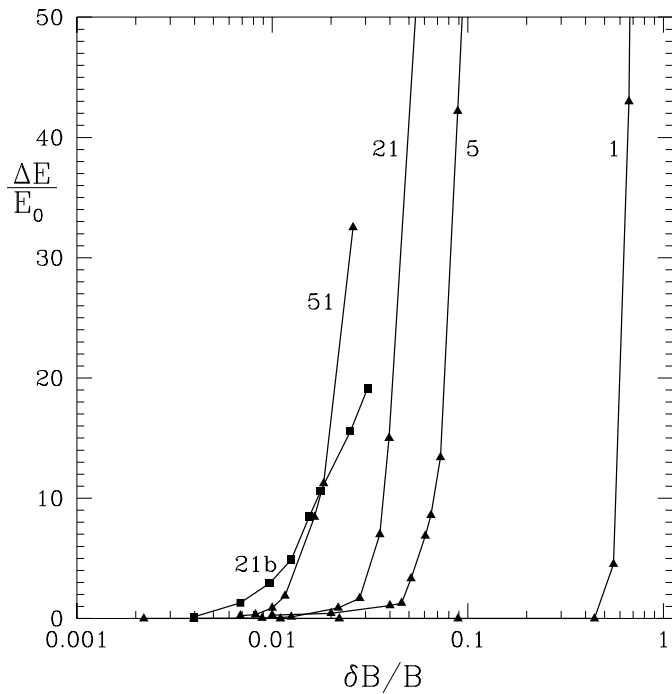


Fig. 14. Stochastic heating due to a spectrum of Alfvén waves.

External Distribution

Plasma Research Laboratory, Australian National University, Australia
Professor I.R. Jones, Flinders University, Australia
Professor João Canalle, Instituto de Fisica DEQ/IF - UERJ, Brazil
Mr. Gerson O. Ludwig, Instituto Nacional de Pesquisas, Brazil
Dr. P.H. Sakanaka, Instituto Fisica, Brazil
The Librarian, Culham Laboratory, England
Library, R61, Rutherford Appleton Laboratory, England
Mrs. S.A. Hutchinson, JET Library, England
Professor M.N. Bussac, Ecole Polytechnique, France
Librarian, Max-Planck-Institut für Plasmaphysik, Germany
Jolan Moldvai, Reports Library, MTA KFKI-ATKI, Hungary
Dr. P. Kaw, Institute for Plasma Research, India
Ms. P.J. Pathak, Librarian, Institute for Plasma Research, India
Ms. Clelia De Palo, Associazione EURATOM-ENEA, Italy
Dr. G. Grosso, Instituto di Fisica del Plasma, Italy
Librarian, Naka Fusion Research Establishment, JAERI, Japan
Library, Plasma Physics Laboratory, Kyoto University, Japan
Research Information Center, National Institute for Fusion Science, Japan
Dr. O. Mitarai, Kyushu Tokai University, Japan
Library, Academia Sinica, Institute of Plasma Physics, People's Republic of China
Shih-Tung Tsai, Institute of Physics, Chinese Academy of Sciences, People's Republic of China
Dr. S. Mirnov, TRINITI, Troitsk, Russian Federation, Russia
Dr. V.S. Strelkov, Kurchatov Institute, Russian Federation, Russia
Professor Peter Lukac, Katedra Fyziky Plazmy MFF UK, Mlynska dolina F-2, Komenskeho
Univerzita, SK-842 15 Bratislava, Slovakia
Dr. G.S. Lee, Korea Basic Science Institute, South Korea
Mr. Dennis Bruggink, Fusion Library, University of Wisconsin, USA
Institute for Plasma Research, University of Maryland, USA
Librarian, Fusion Energy Division, Oak Ridge National Laboratory, USA
Librarian, Institute of Fusion Studies, University of Texas, USA
Librarian, Magnetic Fusion Program, Lawrence Livermore National Laboratory, USA
Library, General Atomics, USA
Plasma Physics Group, Fusion Energy Research Program, University of California at San
Diego, USA
Plasma Physics Library, Columbia University, USA
Alkesh Punjabi, Center for Fusion Research and Training, Hampton University, USA
Dr. W.M. Stacey, Fusion Research Center, Georgia Institute of Technology, USA
Dr. John Willis, U.S. Department of Energy, Office of Fusion Energy Sciences, USA
Mr. Paul H. Wright, Indianapolis, Indiana, USA

The Princeton Plasma Physics Laboratory is operated
by Princeton University under contract
with the U.S. Department of Energy.

Information Services
Princeton Plasma Physics Laboratory
P.O. Box 451
Princeton, NJ 08543

Phone: 609-243-2750
Fax: 609-243-2751
e-mail: pppl_info@pppl.gov
Internet Address: <http://www.pppl.gov>